Eur. Phys. J. Plus (2022) 137:1159
https://doi.org/10.1140/epjp/s13360-022-03388-x

THE EUROPEAN PHYSICAL JOURNAL PLUS

Regular Article

First principles study of structural, elastic, electronic, magnetic and thermoelectric properties of ZrRhYZ (Y = Hf, La; Z = Al, Ga, In) quaternary Heusler alloys

R. Meenakshi[2], R. Aram Senthil Srinivasan[3], A. Amudhavalli[4], R. RajeswaraPalanichamy[1,a], K. Iyakutti[5]

[1] Department of Physics, N.M.S.S. Vellaichamy Nadar College, Madurai Kamaraj University, Madurai, Tamilnadu 625019, India
[2] Department of Physics, Government College of Engineering, Tirunelveli, Tamilnadu 627007, India
[3] Department of Basic Science, Government Polytechnic College, Thoothukudi, Tamilnadu 628008, India
[4] Department of Physics, Mannar Thirumalai Naicker College, Madurai Kamaraj University, Madurai, Tamilnadu 625601, India
[5] Department of Physics and Nanotechnology, SRM Institute of Science and Technology, Chennai, Tamilnadu 603203, India

Received: 20 April 2022 / Accepted: 12 October 2022

Abstract The structural, mechanical, electronic structure, magnetic, and thermoelectric properties of ZrRhYZ (Y = Hf, La; Z = Al, Ga, In) quaternary Heusler alloys at normal pressure are studied using first-principles calculations employing density functional theory. The predicted mechanical properties of these alloys show that they are mechanically stable. At normal pressure, the electronic structure of ZrRhYZ (Y = Hf, La; Z = Al, Ga, In) quaternary Heusler alloys suggests that they are half-metallic ferromagnets. In the LiMgPdSn type crystal structure, the alloys ZrRhYZ (Y = Hf, La; Z = Al, Ga, In) have total magnetic moments of 2 μB and 1 μB, respectively, and follow the Slater–Pauling 18-electron-rule. The Seebeck coefficients, electrical conductivity, thermal conductivity, and power factor are calculated using the Boltzmann transport theory at room temperature to understand their thermoelectric properties better.

1 Introduction

First-principles simulations studies predicted various half-metallic Heusler alloys for diverse applications such as thermoelectric devices [1–4], superconductors [5], and spintronic devices [6]. Heusler alloys are typically cubic in structure and contain four atoms. The four atoms are positioned in the Wyckoff co-ordinates: X (0, 0, 0), X' (1/2, 1/2, 1/2), Y (1/4, 1/4, 1/4), and Z (3/4, 3/4, 3/4). In line with occupational atoms, Heusler compounds have numerous structure types, such as full Heusler, half-Heusler, inverse-Heusler, and quaternary Heusler.

Quaternary Heusler alloys form a non-centrosymmetric cubic structure with the space group F-43 m (space group no-216). Quaternary Heusler alloys have a crystal structure that is similar to that of cubic LiMgPdSn [7] and are identified by the formula $XX'YZ$, where X, X', and Y are transition metals, and Z is the main group element. The LiMgPdSn crystal structure is made up of four interpenetrating fcc sub-lattices and four distinct crystal sites: X (0, 0, 0), X' (1/2, 1/2, 1/2), Y (1/4, 1/4, 1/4), and Z (3/4, 3/4, 3/4). The Y atom is situated at one of the two body diagonal positions (1/4, 1/4, 1/4) in the cell, leaving the Z atom at other diagonal positions (3/4, 3/4, 3/4). X and X' atoms form a rock salt structure. The X, X', Y, and Z atoms are located in Wyckoff positions 4a (0, 0, 0), 4b (1/2, 1/2, 1/2), 4c (1/4, 1/4, 1/4), and 4d (3/4, 3/4, 3/4) in the LiMgPdSn structure, also known as the Y type structure.

Heusler alloys containing 4d transition metal gained keen research interest due to their enormous spintronic applications. Shreder et al. [8] investigated the electronic structure, magnetic properties, and optical properties of the Heusler alloys Co_2NiGa, Co_2NiAl, Co_2FeGa, and Co_2FeAl, and demonstrated that Co_2MGa and Co_2MAl alloys with different M atoms are suitable for spintronic applications. Labar et al. [9] examined the structural, mechanical, electrical, magnetic, thermodynamic, and chemical properties of XFeCrAl (X = Rh, Pd, and Pt) equiatomic quaternary Heusler compounds. The electronic structures, mechanical, and thermoelectric characteristics of the quaternary half-metallic Heusler alloys CoFeXSn (X = Ru, Zr, Hf, Ta) were examined by Seh and Gupta [10]. Hoat et al. [11] studied the structural, electronic, magnetic, elastic, and thermodynamic properties of the quaternary Heusler compound CoCrRhSi theoretically. Sicong Jianga and Kesong Yang [12] explored the thermodynamic and lattice dynamical stability of 99 quaternary Heusler alloys with desired features for spintronics and thermoelectric applications. Souheil Belbachir et al. [13] investigated the structural, electrical, magnetic, mechanical, and half-metallic characteristics of quaternary Heusler CoZrFeP using a first-principles approach.

Using a full-potential linearized augmented plane wave (FP-LAPW) technique, Saadi Berri et al. [14] proposed half-metallic ferromagnets ZrCoTiZ (Z = Si, Ge, Ga, and Al) quaternary Heusler alloys. The electronic structures, magnetic, and half-metallic

[a] e-mail: rrpalanichamy@gmail.com (corresponding author)

Published online: 20 October 2022

characteristics of the quaternary Heusler compounds ZrVTiGa and ZrVTiAl with spin-flip gap were explored by Wang et al. [15]. Saadi Berri et al. [16] investigated the structural, electronic, and magnetic properties of quaternary-Heusler alloys ZrNiTiAl, ZrFeTiAl, ZrFeTiGe, and ZrFeTiSi. Qiang Gao et al. [17] found new spin gapless semiconductors in ZrFeCrZ (Z = In and Ga), ZrCoCrBe, ZrCoFeP, ZrFeVGe, and ZrCoVIn quaternary-Heusler alloys by employing first-principle calculations. Da Chai and Shakeel Ahmad Khandy [18] studied the electronic, thermodynamic, magnetic, phonon, and elastic properties of the FeRhCrZ (Z = Si and Ge) quaternary-Heusler alloys based on GGA calculation. Idrissi et al. [19] investigated the electronic and magnetic properties of NbRhCrAl alloy using the FLAPW methods. MONTE CARLO simulations were used to explore the thermal behaviour of the magnetizations and phase diagram of the alloy. Using the full-potential linearized augmented plane wave (FLAPW) approach, Vajiheh Alijani et al. [20] synthesized and theoretically analysed the electronic structure and magnetic characteristics of CoRhMnZ (Z = Ga, Sn, Sb) alloys. Benkabou et al. [21] investigated the electronic structure, magnetic and mechanical properties of CoRhMnZ (Z = Al, Ga, Ge, and Si) Heusler alloys and revealed all these alloys were half-metallic ferromagnets. Yang et al. [22] conducted a study on VCoHfGa and CrFeHfGa by using the GGA + PBE scheme and found that the two alloys are spin gapless semiconductors. Guo et al. [23] investigated the electronic structure and half-metallic properties of ZrFeVZ (Z = Al, Ga and In)quaternary-Heusler alloys containing 4d transition metal exhibiting larger spin-flip band gaps and half-metallic ferrimagnetism. Xie et al. [24] revealed half-metallic ferromagnets in ZrMnVSi, ZrMnVGe, ZrCoFeSi and ZrCoFeGe by full-potential local-orbital (FPLO) minimum-basis band-structure method. Wenbin Liu et al. [25] revealed half-metallic character of ZrRhTiZ (Z = Al, Ga) quaternary Heusler alloys while investigating their electronic, magnetic, and mechanical properties using first-principles calculations. Singh and Gupta [26] investigated the effect of lanthanum on the half-metallic and thermoelectric properties of quaternary lanthanum-based Heusler alloys, LaCoCrGa and LaCoCrAl, using the first-principles method. Wang et al. [27] investigated the electronic structures, magnetic and half-metallic properties of quaternary-Heusler alloys ZrRhHfZ (Z = Al, Ga, In) by employing Plane-wave pseudo-potential methods.

To our knowledge, no comprehensive research of the structural, electrical, and magnetic properties of ZrRhLaAl, ZrRhLaGa, and ZrRhLaIn has been conducted. We have investigated the quaternary-Heusler alloys ZrRhYZ (Y = Hf; Z = Al, Ga, In) at normal pressure using density functional theory (DFT) due to inadequate of research on their structural, elastic, electronic, magnetic, and thermoelectric properties. Since the thermoelectric properties of the quaternary Heusler alloys ZrRhYZ (Y = Hf, La; Z = Al, Ga, In) have yet to be examined, our findings can be used as a framework for new theoretical and experimental research for the fabrication of thermoelectric devices.

2 Theoretical framework

We have theoretically analysed the structural, mechanical, electronic, magnetic, and thermoelectric properties of quaternary-Heusler alloys ZrRhYZ(Y = Hf, La; Z = Al, Ga, In) using Wien2k code [28] based on density functional theory, which applies Full Potential Linearly Augmented Plane Wave (FP-LAPW) [29] method. In our calculations, we employed the Perdew–Burke–Ernzerhof [30, 31] exchange–correlation function to incorporate exchange–correlation effects in the Generalized Gradient Approximation (GGA) method. We used spin-polarized Density Functional Theory in our calculations to account for the role of spin in the geometry optimization of electronic structures. The density of majority and minority spin states is calculated using the Kohn–Sham equations [32]. We took Cut-off energy as − 6 Ry, L-max = 10, RKmax = 8, and G-max = 12 in the calculations. The quaternary Heusler alloys ZrRhYZ (Y = Hf, La; Z = Al, Ga, In) were optimized with the following convergence parameters: $8 \times 8 \times 8$ k-point mesh, 1E-3e charge convergence, and 1E-5Ry energy convergence. The cubic elastic code [33] is used to calculate elastic properties by applying constant hydrostatic pressure in all directions. The Boltzmann transport theory, as established in the BoltzTraP2 code [34], was used to estimate thermoelectric properties using the constant relaxation time and rigid band approximations.

Quaternary Heusler alloys are characterized by the formula $XX'YZ$, with X, X', and Y being transition metals and Z being the main group element. Quaternary Heusler alloys form in the LiMgPdSn type crystal structure with the space group F-43 m (space group no-216), and Wyckoff co-ordinates X (0, 0, 0), X' (1/2, 1/2, 1/2), Y (1/4, 1/4, 1/4), and Z (3/4, 3/4, 3/4). The crystal structure of the ZrRhYZ (Y = Hf, La; Z = Al, Ga, In) quaternary-Heusler alloy is plotted in Fig. 1.

3 Results and discussion

3.1 Structural property

The structural parameters such as lattice constant (a_0), bulk modulus (B), its first pressure derivative (B'), and minimal total energy (E_0) for non-magnetic (NM) and ferromagnetic phases (FM) are determined using the empirical Birch–Murnaghan's equation of states (EOS) [35] by optimizing the volume of the unit cell using the energy minimization approach. The ferromagnetic phase of quaternary-Heusler alloys ZrRhYZ (Y = Hf, La; Z = Al, Ga, In) is shown to be more stable than the non-magnetic phase, as shown in Table 1. The volume optimization curve in non-magnetic and ferromagnetic phases in cubic structures of quaternary-Heusler alloys ZrRhYZ (Y = Hf, La; Z = Al, Ga, In) is shown in Fig. 2.

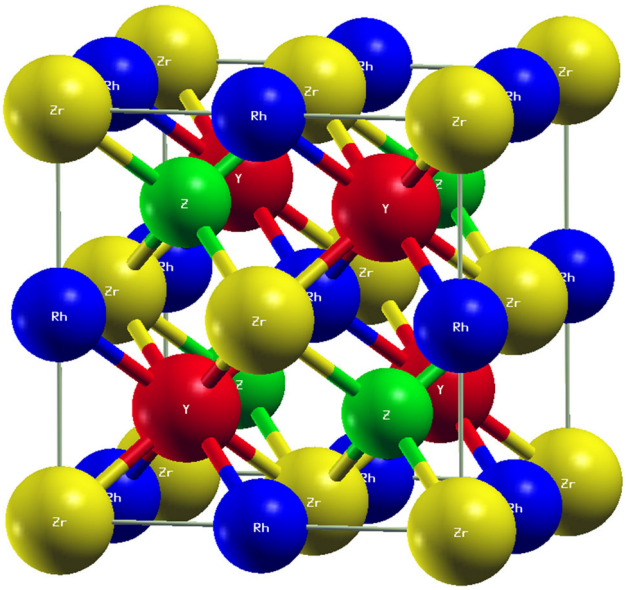

Fig. 1 Crystal structure of ZrRhYZ (Y = Hf, La; Z = Al, Ga, In) quaternary Heusler alloys (space group F-43 m)

Table 1 Calculated lattice parameter a_0 (Å), equilibrium volume V_0(Å^3), total energy E_{Tot} (eV), formation energy E_{f} (eV), bulk modulus B (GPa) and its derivative $B^{'}$ for ZrRhYZ (Y = Hf, La; Z = Al, Ga, In)

Compound	Phase	a_0	V_0	E_{Tot}	E_{f}	B	$B^{'}$
ZrRhHfAl	NM	6.59	483.69	− 645,595.476	− 17.42	129.16	4.63
	FM	6.61	487.73	− 645,595.5397	− 19.46	129.17	4.26
		6.65[a]					
ZrRhHfGa	NM	6.58	481.70	− 691,890.053	− 15.24	140.78	5.77
	FM	6.60	486.16	− 691,890.1135	− 18.37	132.62	4.62
		6.64[a]					
ZrRhHfIn	NM	6.77	523.99	− 58,731.2886	− 16.19	121.44	4.43
	FM	6.79	527.54	− 58,731.2971	− 17.42	123.48	4.38
		6.82[a]					
ZrRhLaAl	NM	6.86	546.01	− 34,249.9996	− 19.05	95.77	3.99
	FM	6.87	545.98	− 34,250.0031	− 20.00	96.09	4.53
ZrRhLaGa	NM	6.83	538.26	− 512,290.0267	− 18.23	98.32	4.51
	FM	6.84	540.20	− 512,290.0578	− 19.04	98.18	4.43
ZrRhLaIn	NM	7.02	585.41	− 45,530.9501	− 17.42	89.86	4.44
	FM	7.04	587.60	− 45,530.9536	− 31.02	88.70	4.38

[a]Ref. [27] Theo

The formation energy (E_{f}) of alloys determines phase stability and whether or not these alloys may be made experimentally. The formula for calculating formation energy is

$$E_{\text{f}} = E_{\text{total}}^{XX^{'}YZ} - \left[E_{\text{bulk}}^{X} + E_{\text{bulk}}^{X^{'}} + E_{\text{bulk}}^{Y} + E_{\text{bulk}}^{Z}\right]$$

It is found that the ZrRhYZ (Y = Hf, La; Z = Al, Ga, In) quaternary Heusler alloys have negative formation energies. This suggests that these alloys can be easily synthesized at ambient conditions.

The cubic structure of the quaternary Heusler alloys ZrRhYZ (Y = Hf, La; Z = Al, Ga, In) includes three elastic constants, C_{11}, C_{12}, and C_{44}. We used the IRelast package, which was interfaced with theWien2k code, to calculate elastic constants. Elastic moduli, Strength, Poisson's ratio, melting temperature, sound velocities, and Debye temperature are all mechanical properties provided by these elastic constants. To assess the mechanical properties of alloys for stability, the Born–Haung criteria [36] have been used. The elastic constants in Table 2 meet the stability criterion, indicating that the quaternary Heusler alloys ZrRhYZ (Y = Hf, La; Z = Al, Ga, In) are mechanically stable in the LiMgPdSn type crystal structure. Brittleness and ductility for a cubic material are determined using the B/G value [37] and Cauchy's pressure. If the B/G value is less than 1.75, the material is brittle. Furthermore, if the B/G value is larger than1.75, the material is ductile. The negative Cauchy's pressure values for a cubic material imply brittle behaviour, whereas the positive Cauchy's pressure values suggest ductile behaviour. Both the B/G value and Cauchy's pressure values indicate

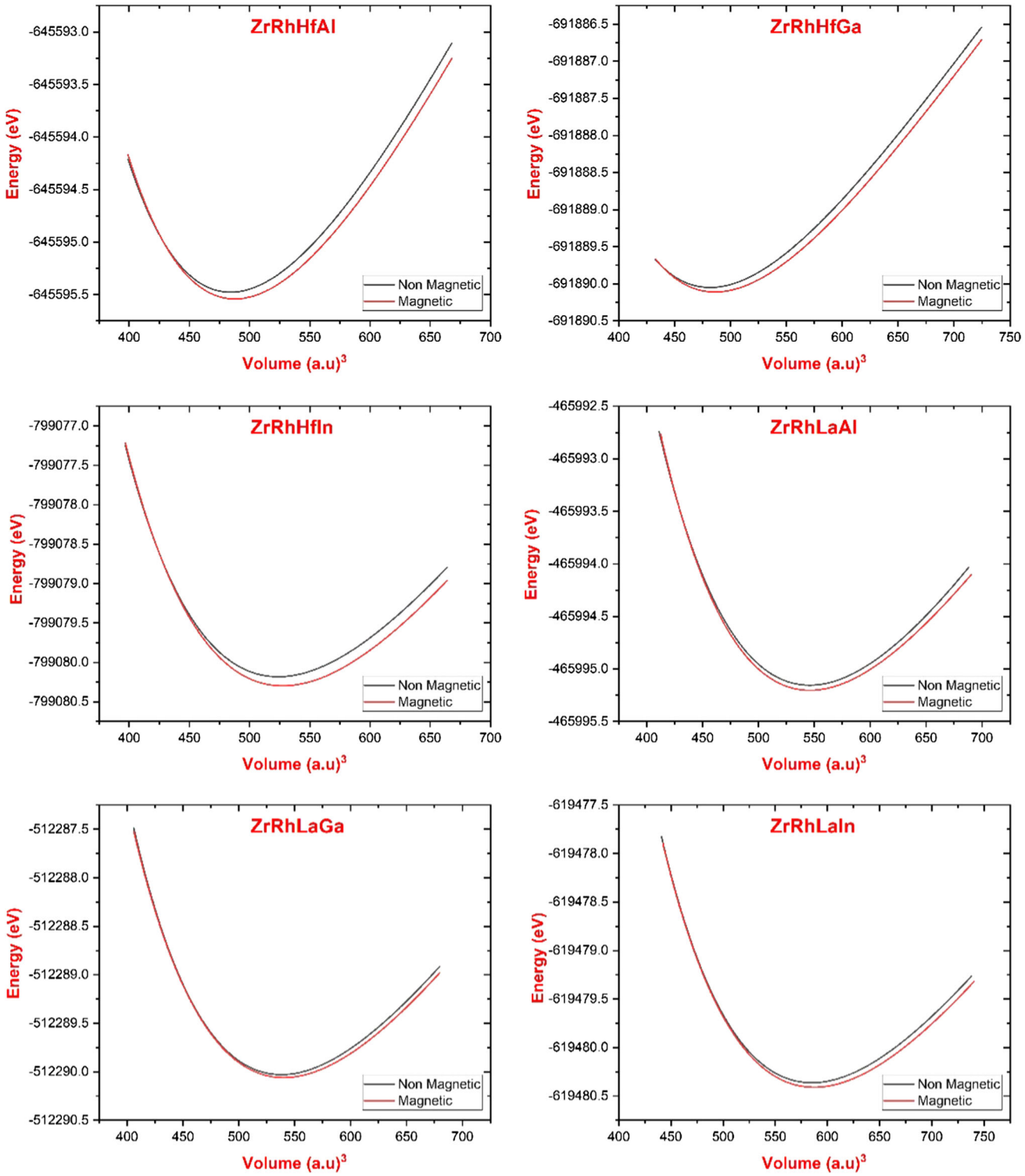

Fig. 2 Total energy (in Ry) optimization variation versus volumes (in a.u^3) for the ZrRhYZ (Y = Hf, La; Z = Al, Ga, In) quaternary Heusler alloys

that these alloys are ductile. The anisotropy factor A values of ZrRhYZ (Y = Hf, La; Z = Al, Ga, In) alloys are found to differ from unity, implying anisotropic elastic behaviour. Table 3 shows the calculated molecular mass, density, Debye temperature, velocities, melting temperature and Curie temperature. The maximum melting temperature and Curie temperature for ZrRhHfIn alloy have been observed in quaternary Heusler alloys ZrRhYZ (Y = Hf, La; Z = Al, Ga, In).

Table 2 Calculated elastic constants C_{ij} (GPa), Voigt–Reuss–Hill bulk modulus B (GPa), shear modulus G (GPa), B/G ratio, G/B ratio, Young's modulus E (GPa), Poisson's ratio ν, Cauchy's pressure C_p (GPa) and Zener anisotropy parameter A of ZrRhYZ (Y = Hf, La; Z = Al, Ga, In)

Compound	C_{11} (GPa)	C_{12} (GPa)	C_{44} (GPa)	B (GPa)	G (GPa)	B/G	G/B	E (GPa)	ν	C_p (GPa)	A
ZrRhHfAl	152.05	113.95	72.97	126.65	42.81	2.96	0.34	115.44	0.34	40.97	3.83
ZrRhHfGa	144.90	120.51	71.53	128.64	36.03	3.57	0.28	98.88	0.37	48.98	5.86
ZrRhHfIn	162.53	139.99	80.13	147.51	37.92	3.89	0.26	104.78	0.38	59.87	7.11
ZrRhLaAl	124.95	79.41	51.69	94.59	37.19	2.54	0.39	98.66	0.32	27.72	2.27
ZrRhLaGa	124.63	81.21	47.49	95.68	34.68	2.76	0.36	92.84	0.33	33.72	2.19
ZrRhLaIn	117.25	72.33	43.26	87.31	33.24	2.625	0.38	88.50	0.33	29.08	1.93

Table 3 Calculated mass M (g/mol), density ρ (g/cm^3), longitudinal v_l (m/s), transverse v_t (m/s), average elastic wave velocity v_m (m/s), Debye temperature θ_D, Melting Temperature T_m (K) and Curie temperature (K) of ZrRhYZ (Y = Hf, La; Z = Al, Ga, In)

Compound	Mass	ρ (g/cm^3)	v_l (m/s)	v_t (m/s)	v_m (m/s)	θ_D (K)	T_m (K)	T_c (K)
ZrRhHfAl	399.60	0.82	2164.59	4483.95	2433.04	275.62	1451.63	491.26
ZrRhHfGa	442.34	0.91	1879.83	4162.34	2119.81	240.79	1409.36	468.52
ZrRhHfIn	487.44	0.92	1914.83	4376.23	2162.16	238.89	1513.52	894.31
ZrRhLaAl	360.02	0.66	2243.72	4417.45	2514.65	274.78	1291.45	377.16
ZrRhLaGa	402.76	0.75	2037.59	4121.7	2287.3	250.83	1289.58	240.31
ZrRhLaIn	447.86	0.76	1973	3925.87	2212.67	235.93	1245.93	363.05

3.2 Electronic properties

At normal pressure, the spin-resolved total, the partial density of states (DOS), and electronic band structures of quaternary-Heusler alloys ZrRhYZ (Y = Hf, La; Z = Al, Ga, In) are computed to examine their electronic structure. Figure 3 shows the spin-resolved total density of states (DOS) of quaternary-Heusler alloys ZrRhYZ (Y = Hf, La; Z = Al, Ga, In) at normal pressure. The majority spin (spin-up) state of quaternary-Heusler alloys ZrRhYZ (Y = Hf, La; Z = Al, Ga, In) exhibits metallic property, whereas the minority spin (spin-down) channel exhibits semiconducting property. Table 4 shows the predicted band gap of quaternary-Heusler alloys ZrRhYZ (Y = Hf, La; Z = Al, Ga, In) alloys at normal pressure. Other theoretical research has reported energy gaps of 0.5596 eV for ZrRhHfAl, 0.743 eV for ZrRhHfGa, and 0.67 eV for ZrRhHfIn. The band gap values for the quaternary Heusler alloys ZrRhHfAl, ZrRhHfGa, and ZrRhHfIn differ due to the use of different exchange correlation functions in the computation. The d-states of atoms Zr, Rh, and Hf play a crucial role in bonding and anti-bonding regions in both spin-up and spin-down channels in all ZrRhHfZ (Z = Al, Ga, In) quaternary Heusler alloys. Figure 4 shows spin-resolved PDOS profile shows that there is a substantial interaction between the d-states of Zr, Rh, and Hf atoms at normal pressure close to the Fermi level. It is clearly observed from Fig. 3 that the spin-up channel is metallic, and the spin-down channel is half-metallic with a small bandgap. The spin-resolved PDOS profile shown in Fig. 4 for ZrRhLaZ (Z = Al, Ga, In) quaternary Heusler alloys displays an interaction between d-states of Zr and Rh, and f states of La atoms at normal pressure near to the Fermi level.

3.3 Magnetic properties

The magnetic characteristics of ZrRhYZ (Y = Hf, La; Z = Al, Ga, In) quaternary Heusler alloys are investigated using spin polarized computations. The electron spin-polarization is determined at the Fermi level using the formula as follows [38]:

$$P = \frac{\rho \uparrow (E_F) - \rho \downarrow (E_F)}{\rho \uparrow (E_F) + \rho \downarrow (E_F)}$$

where $\rho \uparrow (E_F)$ is the majority spin, and $\rho \downarrow (E_F)$ is the minority spin of the density of state at Fermi level. The percentage of spin polarization has been computed using the aforementioned formula, and ZrRhYZ (Y = Hf, La; Z = Al, Ga, In) alloys possess 100% spin polarization, satisfying the half-metallic characteristic.

Table 4 shows the total magnetic moment (B) of ZrRhYZ (Y = Hf, La; Z = Al, Ga, In) quaternary Heusler alloys. The most considerable contributions to the net moment are clearly seen to come from the atoms Zr and Hf. The intense localized spin moment at the Zr and Hf atoms' sites is owing to large d state exchange splitting. When the atomic magnetic moments of the Zr and Hf atoms are compared, we discover that they are aligned in the same direction. The quaternary Heusler alloys ZrRhYZ (Y = Hf, La; Z = Al, Ga, In) is a half-metallic ferromagnet.

Furthermore, in all ZrRhYZ (Y = Hf, La; Z = Al, Ga, In) alloys, the interstitial region contributes a significant amount to the magnetic moment. Because the majority of the d states exist in the muffin-tin spheres of the Zr, Rh, and Hf elements, d–d hybridization occurs mostly inside muffin-tin spheres, resulting in an increase in magnetic moments in the interstitial area.

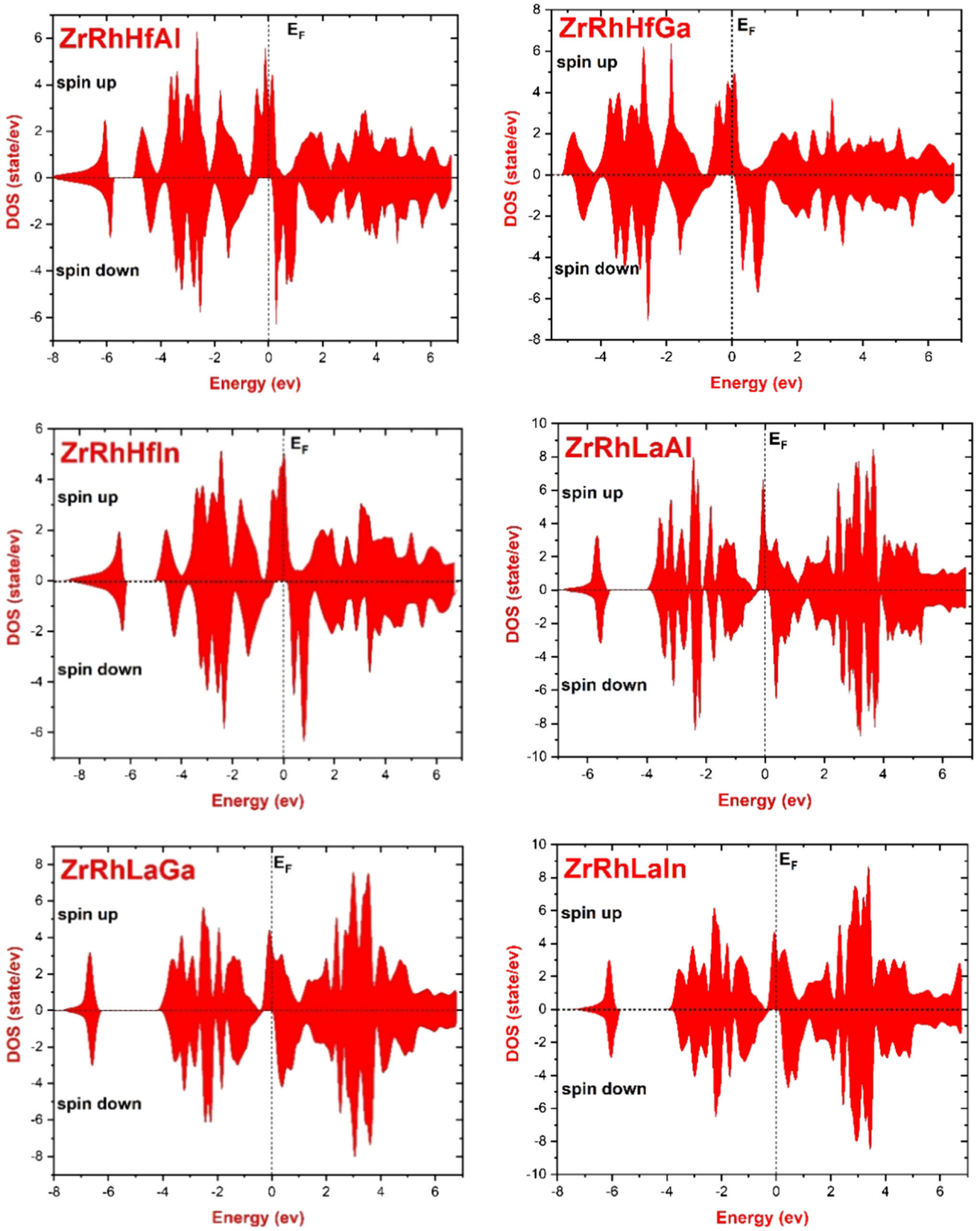

Fig. 3 Total density of states (DOS) of ZrRhYZ (Y = Hf, La; Z = Al, Ga, In) quaternary Heusler alloys at normal pressure

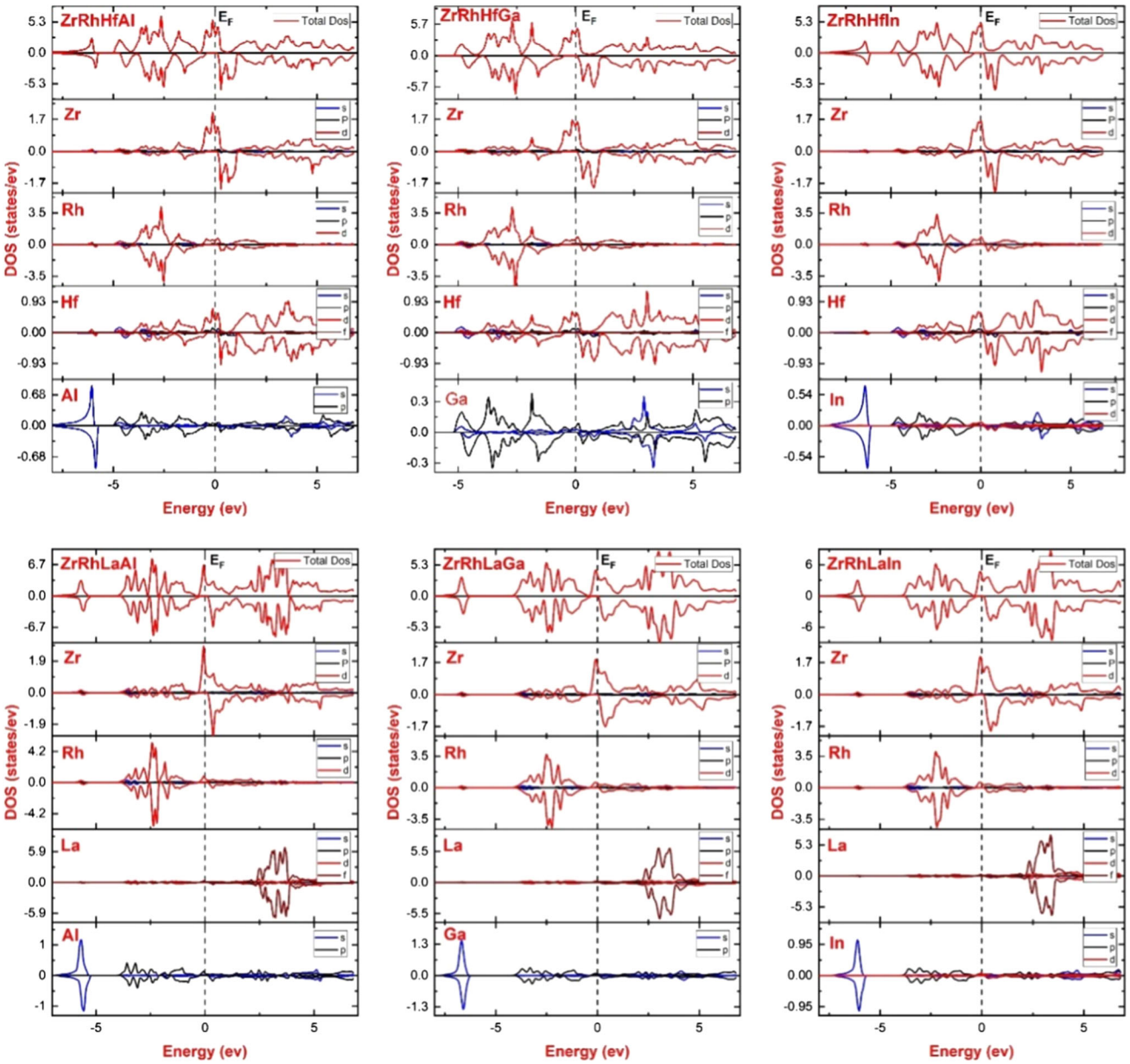

Fig. 4 Partial density of states (PDOS) of ZrRhYZ (Y = Hf, La; Z = Al, Ga, In) quaternary Heusler alloys at normal pressure

The Slater–Pauling 18-electron-rule is used to investigate the magnetic behaviour of quaternary Heusler alloys. The total magnetic moment is calculated using this rule in terms of the atomic number, i.e. $M_{\mathrm{Tot}} = Z_{\mathrm{Tot}} - 18$ [39, 40], where Z_{Tot} denotes the total number of valence electrons. The total magnetic moment of ZrRhYZ (Y = Hf, La; Z = Al, Ga, In) quaternary Heusler alloys is 2 μB and 1 μB, respectively, with 20 and 19 valence electrons per unit cell. The computed magnetic moment values for ZrRhYZ quaternary Heusler alloys (Y = Hf, La; Z = Al, Ga, In) coincide with the Slater–Pauling rule.

The existence of ferromagnetism in ZrRhYZ (Y = Hf, La; Z = Al, Ga, In) quaternary Heusler alloys can also be evaluated by the Stoner criterion which states:

$$IN(E_{\mathrm{f}}) > 1$$

where I is the Stoner parameter and $N(E_{\mathrm{f}})$ is the density of states at the Fermi level in the non-magnetic phase. The Stoner parameter is obtained from the following definition:

$$\Delta_{\mathrm{ex}} = Im$$

Table 4 Calculated total magnetic moment (μ_{Total} in μ_B) per unit cell and the local magnetic moment of each site, band gaps (eV) and the spin-polarization at the Fermi level of ZrRhYZ (Y = Hf, La; Z = Al, Ga, In)

Compound	μ_{Zr}	μ_{Rh}	μ_Y	μ_Z	μ_{int}	μ_{Tot}	E_g	P %
ZrRhHfAl	1.147	0.129	0.332	0.010	0.377	1.999	0.494	100
	1.54[a]	− 0.06[a]	0.62[a]	− 0.1[a]		2[a]	0.5596[a]	100
ZrRhHfGa	1.126	0.117	0.392	0.004	0.361	2.000	0.557	100
	1.46[a]	− 0.06[a]	0.76[a]	− 0.16[a]		2[a]	0.743[a]	100
ZrRhHfIn	1.101	0.0856	0.402	0.006	0.406	2.001	0.562	100
	1.46[a]	− 0.08[a]	0.79[a]	− 0.16[a]		2[a]	0.67[a]	100
ZrRhLaAl	0.549	0.056	0.079	0.029	0.282	0.995	0.298	100
ZrRhLaGa	0.546	0.069	0.092	0.017	0.275	0.999	0.392	100
ZrRhLaIn	0.569	0.044	0.089	0.007	0.292	1.001	0.415	100

[a]Ref. [27] Theo

Table 5 Calculated total magnetic moment (m in μ_B) per unit cell, the exchange splitting (Δ_{ex}ineV), the Stoner parameter (I in eV/μ_B), total density of states at the Fermi level for the non-magnetic case ($N(E_f)$) and $IN(E_f)$ of ZrRhYZ (Y = Hf, La; Z = Al, Ga, In)

Compound	m	Δ_{ex}	I	$N(E_f)$	$IN(E_f)$
ZrRhHfAl	0.499	0.408	0.817	3.408	2.783
ZrRhHfGa	0.5	0.245	0.489	4.190	2.053
ZrRhHfIn	0.5	0.408	0.816	5.045	4.119
ZrRhLaAl	0.249	0.435	1.750	4.344	7.603
ZrRhLaGa	0.249	0.463	1.852	3.739	6.927
ZrRhLaIn	0.25	0.463	1.850	4.089	7.566

where Δ_{ex}, the exchange splitting, is the band splitting between spin up and spin down channel due to magnetization. The exchange splitting is calculated directly from the total DOS of the ZrRhYZ (Y = Hf, La; Z = Al, Ga, In) quaternary Heusler alloys. m is the total magnetic moment per atom. Table 5 lists the total DOS at the Fermi level $N(E_f)$ and the exchange integrals (I), and their products ($IN(E_f)$) of ZrRhYZ (Y = Hf, La; Z = Al, Ga, In) quaternary Heusler alloys. Table 5 shows that the products ($IN(E_f)$) of ZrRhYZ (Y = Hf, La; Z = Al, Ga, In) quaternary Heusler alloys are greater than one, indicating that the Stoner criterion is fulfilled. The results show that these alloys are in magnetic ground states.

Curie temperature is the temperature at which certain magnetic materials lose all of their magnetic properties and undergo a sharp change in their magnetic properties. We estimate the Curie temperature T_C for ZrRhYZ (Y = Hf, La; Z = Al, Ga, In) quaternary Heusler alloys using the mean field approximation (MFA) [41] by neglecting the spin change as

$$T_C = \frac{2\Delta E}{3K_B}$$

where K_B is the Boltzmann constant and ΔE is the total energy difference between the non-magnetic and ferromagnetic phases. Table3 shows the estimated Curie temperature T_C for ZrRhYZ (Y = Hf, La; Z = Al, Ga, In) quaternary Heusler alloys. ZrRhHfIn has the highest estimated T_C value, followed by ZrRhHfAl, ZrRhHfGa, ZrRhLaAl, ZrRfLaIn, and ZrRhLaGa. The high Curie temperature [42] of Heusler alloys makes them suitable for spintronics and thermoelectric applications.

3.4 Thermoelectric properties

The Boltzmann transport theory, as implemented in the BoltzTraP2 algorithm with the constant relaxation time and rigid band approximations, was used to analyse thermoelectric properties. The thermoelectric properties of ZrRhYZ (Y = Hf, La; Z = Al, Ga, In) alloys, such as Seebeck coefficient, electrical and thermal conductivities, and Power factor, have been computed. At room temperature, the calculated thermoelectric characteristics of ZrRhYZ (Y = Hf, La; Z = Al, Ga, In) alloys were displayed as a function of the chemical potential.

Half metallic ferromagnetism is observed in ZrRhYZ (Y = Hf, La; Z = Al, Ga, In) quaternary Heusler alloys. For semiconductors, the Seebeck coefficient is around 100 times higher than for metals [43]. The Seebeck coefficient is used to test the electronic structure of alloys in the Fermi energy region. We have plotted the Seebeck coefficient (S) as a function of chemical potential (μ), which is equivalent to Fermi energy at 0 K, in Fig. 5 [34, 44].

Figure 5 shows the computed Seebeck coefficients as a function of chemical potential (μ) at room temperature. In the semiconducting state, $\mu = 0$ corresponds to the top of the valence band [45]. Because the majority spin channel acts metal, a lower S value is expected when compared to the S value for the minority spin channel. For the minority spin channel, there are two peaks near $\mu = 0$; a negative value of S dominates n-type behaviour, whereas a positive value indicates p-type behaviour in the system [46–51]. Table 6 shows the peaks of Seebeck coefficients in the p-type and n-type regions for ZrRhYZ (Y = Hf, La; Z = Al, Ga, In) alloys at chemical potentials ranging from 0.02 to − 0.02 eV. The Seebeck coefficient exhibits substantial values in both the p-type and n-type regions, indicating that both carrier types may be present.

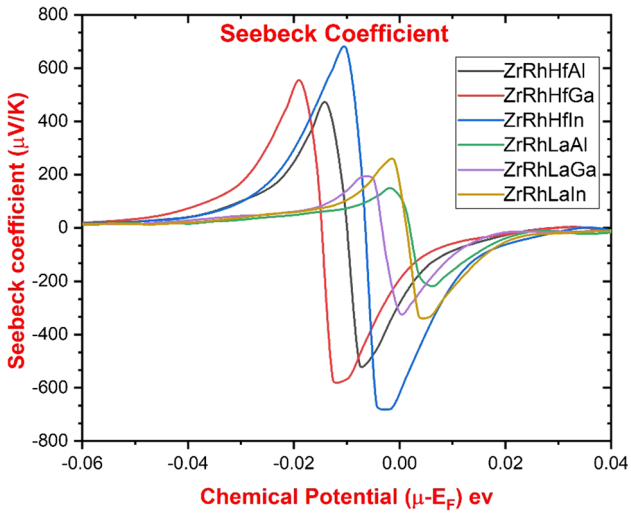

Fig. 5 The Seebeck coefficient (S) as a function of the chemical potential corresponding to shifting of the Fermi energy at room temperature for ZrRhYZ (Y = Hf, La; Z = Al, Ga, In) quaternary Heusler alloys

Table 6 Maximum values of Seebeck coefficient S (μV/K); Electrical conductivity σ (10^{20}/Ωms); thermal conductivity κ (10^{15}w/mk^2 s) and power factor per relaxation time (10^{11}) of ZrRhYZ (Y = Hf, La; Z = Al, Ga, In)

Compound	*p*-Type				*n*-Type			
	S	σ	κ	PF	S	σ	κ	PF
ZrRhHfAl	464	4.99	3.57	3.36	− 512	2.41	1.74	3.99
ZrRhHfGa	546	4.67	3.33	2.97	− 569	3.01	1.99	3.35
ZrRhHfIn	669	4.26	3.04	3.16	− 678	2.86	1.8	3.62
ZrRhLaAl	227	4.26	3.05	1.60	− 219	3.01	2.09	5.74
ZrRhLaGa	190	3.55	2.55	1.53	− 317	2.90	2.03	6.91
ZrRhLaIn	252	4.04	2.87	1.89	− 333	2.47	1.72	6.20

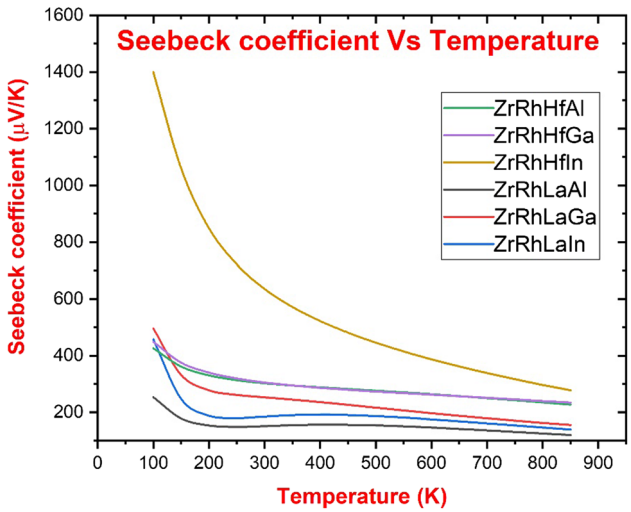

Fig. 6 The variation of Seebeck coefficient (S) with temperature for ZrRhYZ (Y = Hf, La; Z = Al, Ga, In) quaternary Heusler alloys

Figure 6 displays the temperature dependence of the Seebeck coefficient of the ZrRhYZ (Y = Hf, La; Z = Al, Ga, In) quaternary Heusler alloys. It demonstrates that when the temperature rises, the absolute values of the Seebeck coefficient in all of these alloys decrease. The ZrRhHfIn alloy has the most significant Seebeck coefficient in ZrRhYZ (Y = Hf, La; Z = Al, Ga, In) alloys.

The interdependencies between the carrier concentration and the Seebeck coefficient are determined by the electron transport model for metals and semiconductors. The Seebeck coefficient is defined by

$$S = \frac{8\pi^2 k_B^2}{3eh^2} m^* T \left(\frac{\pi}{3n}\right)^{3/2}$$

where m^* is the effective mass of the carrier and n is the carrier concentration. It is obvious that the Seebeck coefficient depends on the concentration of the carrier and the effective mass m^*. The Seebeck coefficient falls with increasing carrier concentration in ZrRhYZ (Y = Hf, La; Z = Al, Ga, In) quaternary Heusler alloys [52]. Furthermore, the values drop with increasing temperature

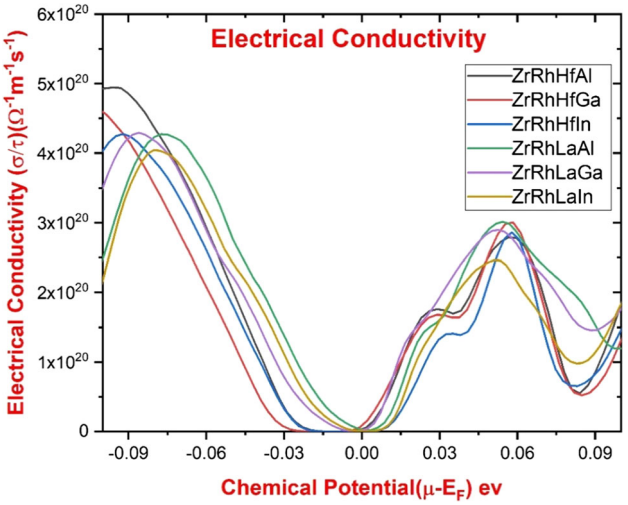

Fig. 7 The electrical conductivity (σ) as a function of the chemical potential corresponding to shifting of the Fermi energy at room temperature for ZrRhYZ (Y = Hf, La; Z = Al, Ga, In) quaternary Heusler alloys

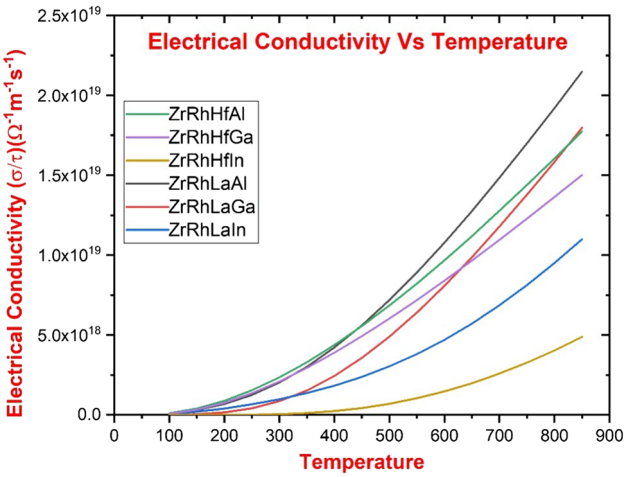

Fig. 8 The variation of electrical conductivity (σ) with temperature for ZrRhYZ (Y = Hf, La; Z = Al, Ga, In) quaternary Heusler alloys

until they reach the Curie temperature, beyond which they remain almost constant [53]. Moreover, Fig. 6 shows that the Seebeck coefficient is dramatically influenced when the electronic structure is significantly altered while undergoing the ferromagnetic to paramagnetic phase transition around Curie temperature. In comparison to ZrRhLaAl, ZrRhLaGa, ZrRhLaIn, the Curie temperature and Seebeck coefficient of ZrRhHfAl, ZrRhHfGa, and ZrRhHfIn were considered to be good.

The Seebeck coefficient links thermal and electrical conductivity, which estimates thermoelectric performances of materials. Figure 7 shows the predicted electrical conductivities for ZrRhYZ (Y = Hf, La; Z = Al, Ga, In) alloys against the chemical potential at 300 K. The electrical conductivity of these alloys is lowest at zero chemical potential and increases as the chemical potential is increased, as seen in Fig. 7. In the negative chemical potential region, electrical conductivity is higher than in the positive region. Table 6 shows the highest values of electrical conductivities for ZrRhYZ (Y = Hf, La; Z = Al, Ga, In) alloys. Among the ZrRhYZ (Y = Hf, La; Z = Al, Ga, In) alloys, the ZrRhHfAl alloy has the highest electrical conductivity of $5 \times 10^{20}/\Omega$ms. Figure 8 depicts the electrical conductivities of ZrRhYZ (Y = Hf, La; Z = Al, Ga, In) alloys as a function of temperature for the minority spin channel at the Fermi level. When the temperature rises above 300 K, the electronic conductivity increases.

The electronic thermal conductivities of ZrRhYZ (Y = Hf, La; Z = Al, Ga, In) alloys are plotted against the chemical potential at 300 K and summarized in Table5, where the thermal conductivity is lowest at zero chemical potential. Because thermal conductivities are at their lowest in the chemical potential range − 0.03 and 0.03 eV, these alloys produce a good thermo-electric response, as seen in Fig. 9. The calculated thermal conductivity has the same behaviour as the electrical conductivity because the maximum points of thermal conductivity exist on the same chemical potential value as the maximum points of electrical conductivity, proving the Widemann–Franz law, which states that the thermal conductivity has the same behaviour as the electrical conductivity [54]. The fluctuation of the electronic thermal conductivity with temperature for the minority spin channel is plotted in Fig. 10. It is worth noting that electrical, thermal conductivity increases slightly as the temperature rises.

The Seebeck coefficient and electrical conductivity information are used to calculate the power factor (PF = $S^2\sigma/\tau$). Another significant component in determining a material's figure of merit is the power factor. Figure 11 shows the power factors for ZrRhYZ (Y = Hf, La; Z = Al, Ga, in) alloys at 300 K as a function of chemical potential between − 0.06 and 0.06 eV. The power factor is

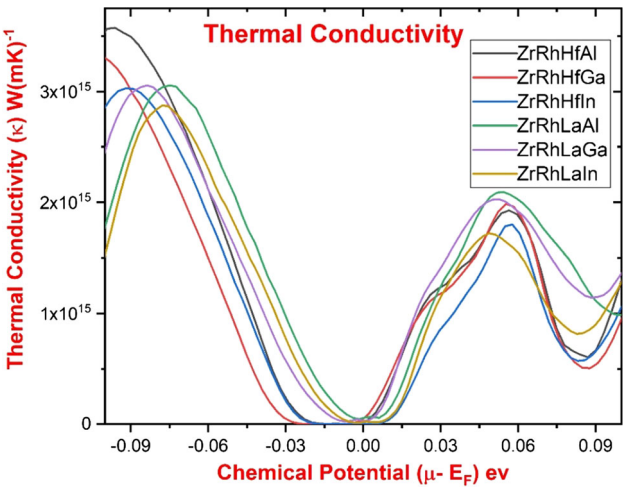

Fig. 9 The electronic thermal conductivity (κ_e) as a function of the chemical potential corresponding to shifting of the Fermi energy at room temperature for ZrRhYZ (Y = Hf, La; Z = Al, Ga, In) quaternary Heusler alloys

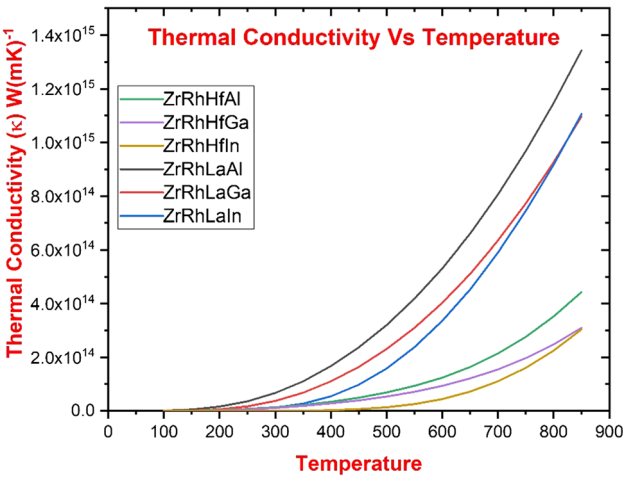

Fig. 10 The variation of thermal conductivity (κ_e) with temperature for ZrRhYZ (Y = Hf, La; Z = Al, Ga, In) quaternary Heusler alloys

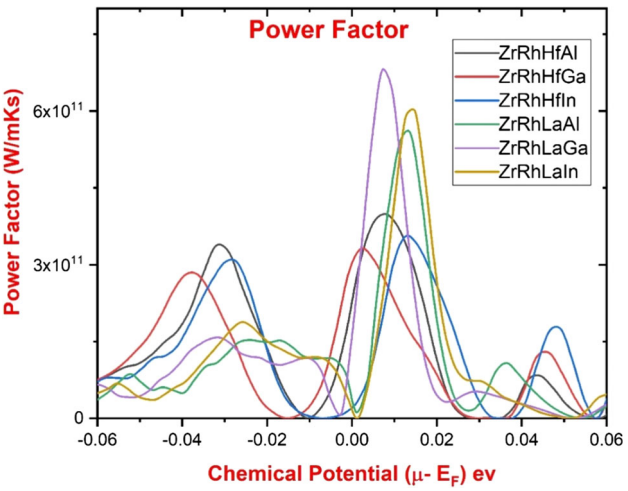

Fig. 11 The power factor as a function of the chemical potential corresponding to shifting of the Fermi energy at room temperature for ZrRhYZ (Y = Hf, La; Z = Al, Ga, In) quaternary Heusler alloys

lowest around the Fermi level, and there are two peaks for the *p*-type and *n*-type regions of the alloys beyond that. The findings show that the power factor values for the studied materials' *n*-type region are more significant than those for the *p*-type region. Figure 12 shows the temperature change in the power factors for ZrRhYZ (Y = Hf, La; Z = Al, Ga, In) alloys, which shows that the power factor increases with temperature.

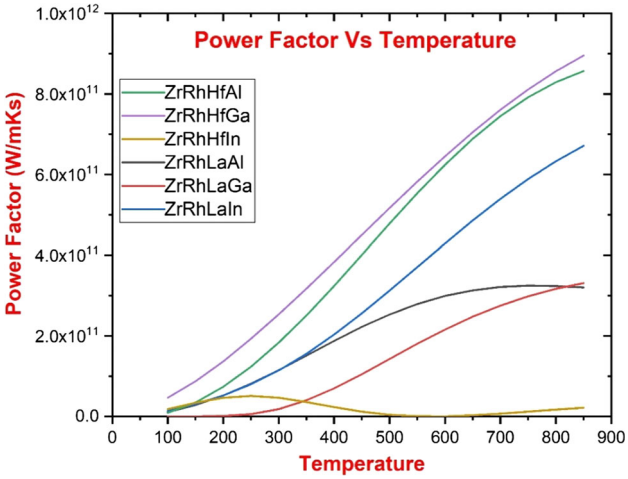

Fig. 12 The variation of power factor with temperature for ZrRhYZ (Y = Hf, La; Z = Al, Ga, In) quaternary Heusler alloys

4 Conclusion

DFT simulations and the semiclassical Boltzmann transport theory are used to examine the structural, electronic, magnetic, and thermoelectric properties of ZrRhYZ (Y = Hf, La; Z = Al, Ga, In) quaternary Heusler alloys. Our findings indicate that quaternary Heusler alloys ZrRhYZ (Y = Hf, La; Z = Al, Ga, In) are most stable in a ferromagnetic state. The computed elastic constant values of these alloys meet all mechanical stability requirements. The DOS and PDOS plots confirm the half-metallic nature of ZrRhYZ (Y = Hf, La; Z = Al, Ga, In) quaternary Heusler alloys. These alloys exhibit indirect band gap in the minority spin channel. The magnetic moment values calculated for ZrRhYZ quaternary Heusler alloys (Y = Hf, La; Z = Al, Ga, In) agree with the Slater–Pauling rule. We have investigated the temperature dependency of thermoelectric properties such as Seebeck coefficient, electrical conductivity, thermal conductivity, and power factor. The existence of *n*-type and *p*-type charge carriers in the alloys is revealed by the positive and negative values of the Seebeck coefficient. The electrical and thermal conductivity of the alloys increases as temperature rises. Except for ZrRhHfIn, the power factor of the alloys increases significantly with increasing temperature. Thus, study shows that the alloys are ideal candidates for applications using spin polarized thermoelectric current because of their fascinating magnetic half metallicity and good thermoelectric characteristics.

Funding The authors declare that no funds, grants, or other support were received during the preparation of this manuscript.

Data availability statement The datasets generated and analysed during the current study are not publicly available due to privacy or ethical restrictions but are available from the corresponding author on reasonable request.

Declarations

Conflict of interest The authors declare that they have no conflict of interest.

References

1. Y. Kimura, Y. Tamura, T. Kita, Appl. Phys. Lett. **92**, 012105 (2008). https://doi.org/10.1063/1.2828713
2. D.P. Rai, Sandeep, A. Shankar, R. Khenata, A.H. Reshak, C.E. Ekuma, R.K. Thapa, S.-H. Ke, AIP Adv. **7**, 045118 (2017). https://doi.org/10.1063/1.4982671
3. B.A. Cook, J.L. Harringa, Z.S. Tan, W. Jesser, in *Proceedings of the ICT'96* (1996), p. 122. https://doi.org/10.1109/ICT.1996.553270
4. C. Kloc, K. Fess, W. Kaefer, K. Friemelt, H. Riazi-Nejad, M. Wendl, E. Bucher, in *Proceedings of the ICT'96* (1996), p. 155. https://doi.org/10.1109/ICT.1996.553281
5. J. Winterlik, G.H. Fecher, A. Thomas, C. Felser, Phys. Rev. B **79**, 064508 (2009). https://doi.org/10.1103/PhysRevB.79.064508
6. K.H.J. Buschow, P.G. Van Engen, J. Magn. Magn. Mater. **25**(1), 90–96 (1981). https://doi.org/10.1016/0304-8853(81)90151-7
7. L. Bainsla, K.G. Suresh, Appl. Phys. Rev. **3**, 031101–031121 (2016). https://doi.org/10.1063/1.4959093
8. E.L. Shreder, A.A. Makhnev, K.G. Suresh, M.G. Kostenko, E.D. Chernov, V.G. Ivanov, A.V. Lukoyanov, Mod. Phys. Lett. B **36**(04), 2150573 (2022). https://doi.org/10.1142/S0217984921505734
9. K. Labar, A. Shankar, M. Ram, A. Laref, R. Sharma, J. Phys. Chem. Solids **156**, 110119 (2021). https://doi.org/10.1016/j.jpcs.2021.110119
10. A.Q. Seh, D.C. Gupta, J. Alloys Compd. **871**, 159560 (2021). https://doi.org/10.1016/j.jallcom.2021.159560
11. D.M. Hoat, D.-Q. Hoang, N.T.T. Binh, M. Naseri, J.F. Rivas-Silva, A.I. Kartamyshev, G.H. Cocoletzi, Mater. Chem. Phys. **257**, 123695 (2021). https://doi.org/10.1016/j.matchemphys.2020.123695
12. S. Jianga, K. Yang, J. Alloys Compd. **867**, 158854 (2021). https://doi.org/10.1016/j.jallcom.2021.158854
13. S. Belbachir, C. Abbes, M.N. Belkaid, A.H. Belbachir, J. Supercond. Nov. Magn. **33**, 2899–2905 (2020). https://doi.org/10.1007/s10948-020-05598-9

14. S. Berri, M. Ibrir, D. Maouche, M. Attallah, Comput. Condens. Matter. **1**, 26–31 (2014). https://doi.org/10.1016/j.cocom.2014.10.003
15. X. Wang, Z. Cheng, J. Wang, L. Wang, Z. Yu, C. Fang, J. Yang, G. Liu, RSC Adv. (2016). https://doi.org/10.1039/C6RA08600D
16. S. Berri, M. Ibrir, D. Maouche, M. Attallah, J. Magn. Magn. Mater. **371**, 106–111 (2014). https://doi.org/10.1016/j.jmmm.2014.07.033
17. Q. Gao, H.H. Xie, L. Li, G. Lei, J.-B. Deng, X.-R. Hu, Superlattices and Microstruct. **85**, 536–542 (2015). https://doi.org/10.1016/j.spmi.2015.05.049
18. S.A. Khandy, J. Chai, J. Appl. Phys. **127**, 165102 (2020). https://doi.org/10.1063/1.5139072
19. S. Idrissia, L. Bahmada, R. Khalladi, I. El Housni, N. El Mekkaoui, S. Mtougui, H. Labrim, S. Ziti, Chin. J. Phys. **60**, 549–563 (2019). https://doi.org/10.1016/j.cjph.2019.05.036
20. V. Alijani, J. Winterlik, G.H. Fecher, S.S. Naghavi, S. Chadov, T. Gruhn, C. Felser, J. Phys. Condens. Matter. **24**, 046001 (2012). https://doi.org/10.1088/0953-8984/24/4/04600
21. M. Benkabou, H. Rached, A. Abdellaoui, D. Rached, R. Khenata, M.H. Elahmar, B. Abidri, N. Benkhettou, S. Bin-Omran, J. Alloys Compd. **647**, 276–286 (2015). https://doi.org/10.1016/j.jallcom.2015.05.273
22. X. Yang, X. Wu, B. Wu, Y. Feng, P. Li, H. Huang, Mater. Sci. Eng. B **209**, 45–50 (2016). https://doi.org/10.1016/j.mseb.2015.12.008
23. R. Guo, G. Liu, X. Wang, H. Rozale, L. Wang, R. Khenata, Z. Wu, X. Dai, RSC Adv. **6**, 109394–109400 (2016). https://doi.org/10.1039/C6RA18873G
24. H.H. Xie, Q. Gao, L. Li, G. Lei, G.Y. Mao, X.R. Hu, J.B. Deng, Comput. Matter. Sci. **103**, 52–55 (2015). https://doi.org/10.1016/j.commatsci.2015.03.010
25. W. Liu, X. Zhang, H. Jia, R. Khenata, X. Dai, G. Liu, Appl. Sci. **9**, 883 (2019). https://doi.org/10.3390/app9050883
26. S. Singh, D.C. Gupta, Results Phys. **13**, 102300 (2019). https://doi.org/10.1016/j.rinp.2019.102300
27. X. Wang, Z. Cheng, R. Guo, J. Wang, H. Rozale, L. Wang, Z. Yu, G. Liu, Mater. Chem. Phys. **193**, 99–108 (2017). https://doi.org/10.1016/j.matchemphys.2017.02.019
28. P. Blaha, K. Schwarz, G.K.H. Madsen, et al. WIEN2k : An augmented plane wave plus local orbitals program for calculating crystal properties. Vienna University of Technology, Austria (2001) (ISBN 39501031-1-2)
29. P. Blaha, K. Schwarz, P. Sorantin, S.B. Trickey, Comput. Phys. Commun. **59**, 399–415 (1990). https://doi.org/10.1016/0010-4655(90)90187-6
30. J.P. Perdew, J.A. Chevary, S.H. Vosko, K.A. Jackson, M.R. Pederson, D.J. Singh, C. Fiolhais, Phys. Rev. B **46**, 6671 (1992). https://doi.org/10.1103/PhysRevB.48.4978.2
31. J.P. Perdew, K. Burke, M. Ernzerhof, Phys. Rev. Lett. **77**, 3865–3868 (1996). https://doi.org/10.1103/physrevlett.77.3865
32. U. Von Barth, L. Hedin, J. Phys. C Solid State Phys. **5**(13), 1629–1642 (1972)
33. M. Jamal, Cubic-elastic (2012) http://www.WIEN2k.at/reg_user/unsupported/cubic-elast/
34. G.K.H. Madsen, D.J. Singh, Comput. Phys. Commun. **175**, 67–71 (2006). https://doi.org/10.1016/j.cpc.2006.03.007
35. F.D. Murnaghan, Proc. Natl. Acad. Sci. USA **30**, 244–247 (1944). https://doi.org/10.1073/pnas.30.9.244
36. M. Born, K. Huang, Dynamical Theory and Experiment, I. Springer, Berlin (1982)
37. S.F. Pugh, Philos. Mag. **45**, 823–843 (1954). https://doi.org/10.1080/14786440808520496
38. R.J. Soulen Jr., J.M. Byers, M.S. Osofsky, B. Nadgorny, T. Ambrose, S.F. Cheng, P.R. Broussard, C.T. Tanaka, J. Nowak, J.S. Moodera, A. Barry, J.M.D. Coey, Science **282**, 85–88 (1998). https://doi.org/10.1126/SCIENCE.282.5386.85
39. I. Galanakis, P.H. Dederichs, N. Papanikolaou, Phys. Rev. B **66**, 174429 (2002). https://doi.org/10.1103/PhysRevB.66.174429
40. K. Özdoğa, E. Şaşıoğlu, I. Galanakis, J. Appl. Phys. **113**, 193903 (2013). https://doi.org/10.1063/1.4805063
41. M.K. Hussain, O.T. Hassan, A.M. Algubili, J. Electron. Mater. (2018). https://doi.org/10.1007/s11664-018-6512-2/
42. T. Graf, C. Felser, S.S.P. Parkin, Prog. Solid. State Chem. **39**(1), 1–50 (2011). https://doi.org/10.1016/j.progsolidstchem.2011.02.001
43. H.C. Kandpal, G.H. Fecher, C. Felser, J. Phys. D Appl. Phys. **40**, 1507 (2007)
44. T. Graf, G.H. Fecher, J. Barth, J. Winterlik, C. Felser, J. Phys. D Appl. Phys. **42**, 084003 (2009)
45. G.H. Fecher, E. Rausch, B. Balke, A. Weidenkaff, C. Felser, Phys. Status Solidi A **213**(3), 716–731 (2016). https://doi.org/10.1002/pssa.201532595
46. D.M. Hoat, M. Naseri, Chem. Phys. **528**, 110510 (2020). https://doi.org/10.1016/j.chemphys.2019.110510
47. A.H. Resha, S. Auluck, Comput. Mater. Sci. **96**, 90–95 (2015). https://doi.org/10.1016/j.commatsci.2014.09.008
48. P.D. Patel, J. Pandya, S.M. Shinde, S. Gupta, S. Narayan, P.K. Jha, Comput. Mater. Sci. **23**, e00472 (2020). https://doi.org/10.1016/j.cocom.2020.e00472
49. E. Pakizeh, J. Jalilian, M. Mohammadi, RSC Adv. **9**, 25900 (2019). https://doi.org/10.1039/c9ra04736k
50. R. Haleoot, B. Hamad, J. Condens. Matter Phys. **32**, 075402 (2019)
51. A. Boudali, A. Mokaddem, B. Doumi, H. Moujri, Acta Phys. Pol. **135**, 409–419 (2019). https://doi.org/10.12693/APhysPolA.135.409
52. G.J. Snyder, E.S. Toberer, Nat. Mater. **7**, 105–114 (2008). https://doi.org/10.1142/9789814317665_0016
53. J. Barth, G.H. Fecher, B. Balke, S. Ouardi, T. Graf, C. Felser, A. Shkabko, A. Weidenkaff, P. Klaer, H.J. Elmers, H. Yoshikawa, S. Ueda, K. Kobayashi, Phys. Rev. B **81**, 064404 (2010). https://doi.org/10.1103/PhysRevB.81.064404
54. A. Reshak, J. Appl. Phys. **117**(22), 225104 (2015). https://doi.org/10.1063/1.4922426